Received: 8 March 2021 | Revised: 31 March 2021 | Accepted: 6 April 2021

DOI: 10.14814/phy2.14848

ORIGINAL ARTICLE

Physiological Reports

High and low expression of the hyperpolarization activated current (I_h) in mouse CA1 stratum oriens interneurons

Lauren T. Hewitt | **Gregory J. Ordemann** | **Darrin H. Brager**

Department of Neuroscience, Institute for Neuroscience, University of Texas at Austin, Austin, TX, USA

Correspondence
Lauren T. Hewitt, Department of Neuroscience, Institute for Neuroscience, University of Texas at Austin, Austin, TX 78712, USA.
Email: laur.hewitt@utexas.edu

Funding information
This work was supported by the National Institutes of Health grant RO1 MH100510 (DHB) and the National Science Foundation Graduate Research Fellowship Program (LTH).

Abstract

Inhibitory interneurons are among the most diverse cell types in the brain; the hippocampus itself contains more than 28 different inhibitory interneurons. Interneurons are typically classified using a combination of physiological, morphological, and biochemical observations. One broad separator is action potential firing: low threshold, regular spiking versus higher threshold, fast spiking. We found that spike frequency adaptation (SFA) was highly heterogeneous in low threshold interneurons in the mouse stratum oriens region of area CA1. Analysis with a k-means clustering algorithm parsed the data set into two distinct clusters based on a constellation of physiological parameters and reliably sorted strong and weak SFA cells into different groups. Interneurons with strong SFA fired fewer action potentials across a range of current inputs and had lower input resistance compared to cells with weak SFA. Strong SFA cells also had higher sag and rebound in response to hyperpolarizing current injections. Morphological analysis shows no difference between the two cell types and the cell types did not segregate along the dorsal–ventral axis of the hippocampus. Strong and weak SFA cells were labeled in hippocampal slices from SST:cre Ai14 mice suggesting both cells express somatostatin. Voltage-clamp recordings showed hyperpolarization activated current I_h was significantly larger in strong SFA cells compared to weak SFA cells. We suggest that the strong SFA cell represents a previously uncharacterized type of CA1 stratum oriens interneuron. Due to the combination of physiological parameters of these cells, we will refer to them as Low Threshold High I_h (LTH) cells.

KEYWORDS

hippocampus, k-means clustering, spike frequency adaptation, voltage-clamp

1 | INTRODUCTION

The elusive classification of the vast number of GABAergic interneuron subtypes has captivated neuroscientists for decades. The laminar organization of the hippocampus makes it an attractive model for studying circuit mechanisms, particularly because hippocampal interneurons have relatively reliable layer specific inputs and outputs (Cobb et al., 1995; Klausberger & Somogyi, 2008; Royer et al., 2012). Hippocampal studies have revealed the extensive diversity of inhibitory interneurons poised to control network timing. Despite comprising merely 10–15% of hippocampal neurons,

the remarkably precise activity of GABAergic inhibitory interneurons controls the timing and specificity of excitatory pyramidal cell output and orchestrates layered levels of synchrony in the hippocampal circuit (reviewed in Bezaire & Soltesz (2013), Freundl & Buzsi (1996), Hájos et al. (2004) and Pelkey et al. (2017)). To this end, interneurons play a critical role in facilitating hippocampal activity that ultimately underly complex hippocampal function such as contextual based learning, the formation of episodic memory, and spatial navigation (Lapray et al., 2012; Lovett-Barron et al., 2014; Murray et al., 2011).

Confident classification of the subtype of GABAergic interneurons is necessary in order to understand the particular role an interneuron plays in the local circuitry. Dissection of the functional roles of different inhibitory neurons has been historically difficult. Many studies utilize a three-part approach that entail describing the morphological, biochemical, and physiological properties (Ascoli et al., 2008; DeFelipe et al., 2013). Within the hippocampus, the CA1 region alone contains at least 28 previously described types of inhibitory interneurons located throughout all layers: stratum oriens, stratum pyramidale, stratum radiatum, and stratum lacunosum-moleculare (Klausberger & Somogyi, 2008). The stratum oriens (SO) of CA1 is home to a variety of regular spiking interneurons, including trilaminar cells, back propagating cells, and oriens-lacunosum moleculare (OLM) cells. OLM cells have a stereotyped morphology with dendrites extending perpendicular to pyramidal cell dendrites along the CA3–subicular axis and an axon that projects through the stratum pyramidale and radiatum until it profusely branches within stratum lacunosum moleculare (Lacaille et al., 1987; Lacaille & Williams, 1990; Maccaferri, 2005; Maccaferri & McBain, 1996). Through this anatomical arrangement, OLM cells coordinate a canonical feedback inhibitory circuit where CA1 neurons activate OLM cells which in turn inhibit the distal dendrites of CA1 pyramidal cells to gate incoming information from the entorhinal cortex via the temporoammonic pathway (Blasco-Ibáñez & Freund, 1995; Klausberger, 2009; Leão et al., 2012; Maccaferri & McBain, 1995; Muller & Remy, 2014). OLM cells exhibit tonic or mildly adapting firings characteristics and display sag and rebound responses during the onset and offset of hyperpolarization due to the expression of h-channels (Lupica et al., 2001; Maccaferri & McBain, 1996). While OLM cells are well characterized, there are many interneurons throughout the brain discovered in patch-seq (Cadwell et al., 2016; Gouwens et al., 2020), single-cell recording (Tricoire et al., 2011), and single cell transcriptomic (Harris et al., 2018) experiments that remain uncharacterized. Descriptions of the subthreshold and active properties, and the ionic condutances that underly them, in these uncharacterized neurons are paramount to understanding how they contribute to the local circuitry.

In the present study, we performed whole-cell recordings from interneurons in the stratum oriens that exhibited oblong cell bodies with dendrites extending along the CA3–subicular axis. We observed heterogeneous spike frequency adaptation (SFA) to depolarizing current injections. Cells with strong SFA also had a lower input resistance, larger voltage sag and steeper rebound in response to hyperpolarizing current injections relative to cells with weak SFA. In contrast, single action potential properties were not correlated with SFA. We measured multiple action potential parameters in tandem with subthreshold properties and used a k-means clustering analysis which parsed the cells into two discrete clusters. Using voltage-clamp recordings, we found cells with strong SFA had larger hyperpolarization activated currents (I_h) compared to cells with weak SFA. We thus suggest the strongly adapting cells are distinct from weak SFA OLM cells. These strong SFA cells exhibit a low-threshold spiking phenotype and will fire action potentials when given small amounts of current relative to other SO interneurons. We will refer to these interneurons as Low-Threshold spiking High I_h cells (LTH).

Our data suggest that OLM and LTH cells exhibit distinct firing and subthreshold properties, which are likely dictated from differences in ion channel and biochemical expression profiles. It is a culmination of ion channel expression, inputs and outputs, and intrinsic physiology that will ultimately dictate how a cell responds to different activity states. It is clear that an appreciation for the highly diverse population of inhibitory interneurons is critical to understanding hippocampal function.

2 | METHODS

2.1 | Slice preparation

All animal procedures were approved by the University of Texas at Austin Institutional Animal Care and Use Committee. All mice were housed in a reverse light–dark cycle of 12 on 12 h off with free access to food and water. Experiments used male wild-type (JAX: C57/Bl6, stock #: 000664) and SST:cre Ai14 mice (JAX: SST:cre (stock #:018973) crossed with Ai14 (stock #: 007914)) 2–4 months old (postnatal day 60—postnatal day 120). Mice were anesthetized with ketamine/xylazine (100/10 mg/kg) and perfused through the heart with ice-cold saline consisting of (in mM): 2.5 KCl, 1.25 NaH_2PO_4, 25 $NaHCO_3$, 0.5 $CaCl_2$, 7 $MgCl_2$, 7 dextrose, 205 sucrose, 1.3 ascorbate, and 3 sodium pyruvate (bubbled with 95% O_2/5% CO_2 to maintain pH at ~7.4). A vibrating tissue slicer (Vibratome 3000, Vibratome Inc.) was used to make 300-μm thick parasagittal sections

from the middle hippocampus. Slices were held in a chamber filled with artificial cerebral spinal fluid (aCSF) consisting of (in mM): 125 NaCl, 2.5 KCl, 1.25 NaH_2PO_4, 25 $NaHCO_3$, 2 $CaCl_2$, 2 $MgCl_2$, 10 dextrose, and 3 sodium pyruvate (bubbled with 95% O_2/5% CO_2) for 30 min at 35°C and then at room temperature until the time of recording.

2.2 | Electrophysiology

Slices were placed in a submerged, heated (33–34°C) recording chamber and continually perfused (1−2 ml/min) with aCSF 125 NaCl, 2.5 KCl, 1.25 NaH_2PO_4, 25 $NaHCO_3$, 2 $CaCl_2$, 2 $MgCl_2$, 10 dextrose, and 3 sodium pyruvate (bubbled with 95% O_2/5% CO_2). Synaptic transmission was blocked with 20 μM DNQX, 25 μM D-AP5, and 2 μM Gabazine. Slices were visualized with a Zeiss AxioScope or Axioexaminer under 60× magnification. All cells were located in the stratum oriens of CA1 and had oblong cell bodies that ran along the subicular–CA3 axis. Experimenters selected cells with oblong cell bodies, smaller than pyramidal cells, with dendrites extending in the CA3–subcircular axis of the SO, perpendicular to pyramidal cell dendrites. Current injections of 100 pA and −80 pA were delivered to determine if the cells physiological properties were consistent with "regular spiking" adapting cells as described in (Maccaferri & McBain, 1996).

2.3 | Current clamp recordings

Internal recording solution contained (in mM): 135 K-gluconate, 10 HEPES, 7 NaCl, 7 K2 phosphocreatine, 0.3 Na−GTP, 4 Mg−ATP (pH 7.3 with KOH). Current clamp data were acquired using a Dagan BVC-700 amplifier with custom acquisition software written using Igor Pro (Wavemetrics) and sampled at 50 kHz, filtered at 3 kHz, and digitized by an ITC-18 (InstruTech) interface. Patch pipettes (4–6 MΩ) were pulled from borosilicate glass. Pipette capacitance was compensated, and the bridge balanced before each recording. Series resistance was monitored throughout each experiment and maintained at approximately 15−35 MΩ. Cells with a series resistance >35 MΩ were omitted from the data set.

2.4 | Voltage clamp recordings

The internal recording solution was the same as for current clamp recordings (see above). Cells were first recorded in control aCSF (see above) in current clamp mode to record trains of action potentials. Following current clamp recording, voltage gated sodium, potassium and calcium currents were blocked with, 1 μM TTX, 10 mM TEA, 5 mM 4AP, 200 μM $BaCl_2$, and 100 μM $CdCl_2$. Cells were held at −30 mV and inward currents were recorded in response to a series of 1-sec long hyperpolarzing voltage commands (−50 to −130 mV in −10 mV steps). Voltage clamp data were acquired using an Axopatch 200B amplifier (Molecular Devices) with Axograph or custom acquisition software written using Igor Pro (Wavemetrics), digitized at 20 kHz and filtered at 3 kHz. Patch pipettes (4–6 MΩ) were pulled from borosilicate glass.

2.5 | Drugs

All drugs (Abcam pharmaceutical or Tocris) were prepared from 1000× stock solutions in water.

2.6 | Post hoc neuron visualization

During whole-cell current clamp recordings, neurons were filled with 0.4% neurobiotin. Upon completion of whole-cell recordings, slices were fixed in 3% paraformaldehyde at 4°C overnight. Slices were then washed with 0.1 M PBS 3× for 20 min and place in a blocking buffer of 10% normal goat serum (NGS) and 0.5% triton in PBS overnight at 4°C. Slices were then incubated in PBS containing 1% BSA and 1% NGS with streptavidin conjugated to Alexa-488 (Invitrogen) for 24–48 h at 4°C. Slices were then rinsed in PBS 3× for 20 min and mounted in Flourmount. Slices were visualized on a resonant scanning 2-photon system (Leica) and Z-stack images were taken. Cells were reconstructed using the max projection of the Z-stack image and analyzed using the SNT plug-in in ImageJ (NIH, https://imagej.net/SNT). (Arshadi et al., 2021).

2.7 | k-means clustering

Neuron properties recorded in current clamp (resting membrane potential, steady-state R_N, max R_N, sag, rebound, ISI ratio, max firing frequency) were used to determine if LTH and OLM cells would separate into distinct populations via k-means clustering. Data were normalized via log transformation and subsequently used for analysis. Using the NbClust package in R (Charrad et al., 2014) we determined the optimal number of clusters for our dataset. We then ran a principal components analysis (PCA) and hierarchical clustering on our data and ultimately determined Euclidean distance using k-means analysis.

2.8 | Data analysis and statistical tests

Electrophysiology data were analyzed using custom analysis software written in IgorPro or AxoGraph. The input

resistance (R_N) was calculated from the linear portion of the current-voltage relationship in response to a family of 1500 ms current injections (−40 pA to +40 pA Δ10 pA). The FI curve was calculated from the number of spikes elicited during a family of 1500 ms depolarizing current injections (25 pA to 250 pA Δ25 pA). All statistical analyses (Student's *t*-test, ANOVA, repeated measures ANOVA, and Pearson's correlation) were performed using Prism (Graphpad).

3 | RESULTS

3.1 | Heterogeneity of spike frequency adaptation in low-threshold regular spiking stratum oriens interneurons

We made whole-cell current clamp recordings from cells in stratum oriens of the CA1 region of the hippocampus with oblong cell bodies and horizontally extending dendrites. Low threshold interneurons were identified by having a resting potential close to action potential threshold, an action potential half-width <1.5 ms, and an initial firing frequency <50 Hz. Stratum oriens interneurons typically display weak to no SFA (Lacaille & Williams, 1990; Maccaferri & McBain, 1996; Williams & Stuart, 2003). Cells were held at −70 mV and depolarizing current injections were used to elicit a train of action potentials. We first measured SFA as the ratio of the last interspike interval (ISI) relative to the first ISI (called the ISI ratio) using the first current step that elicited multiple action potentials (Figure 1a). We found that SFA was highly heterogeneous across cells with some showing weak SFA (ISI close to 1) and others showing strong SFA; the ISI ratio was not correlated with the resting membrane potential. (SFA range across all cells: 1.1–6.5; Pearson's $r = -0.0015$, $p = 0.88$; Figure 1b). While ISI ratio is a reliable indicator of SFA, this method is best when analyzing a single current injection which elicits the same approximate number of action potentials across cells. We therefore sought a second method that would reflect SFA across a range of current injections. Similar to our observation in stratum oriens interneurons, cortical neurons in the piriform cortex display heterogeneous SFA (Barkai & Hasselmo, 1994). Using the same method described in (Barkai & Hasselmo, 1994), we plotted the number of action potentials (spikes) as a function of normalized current injected (Figure 1c). The area under the linear fit is the S-I value, an indication of adaptation strength. In agreement with our measurement of ISI ratio, S-I value was highly heterogeneous across all cells recorded (Figure 1d).

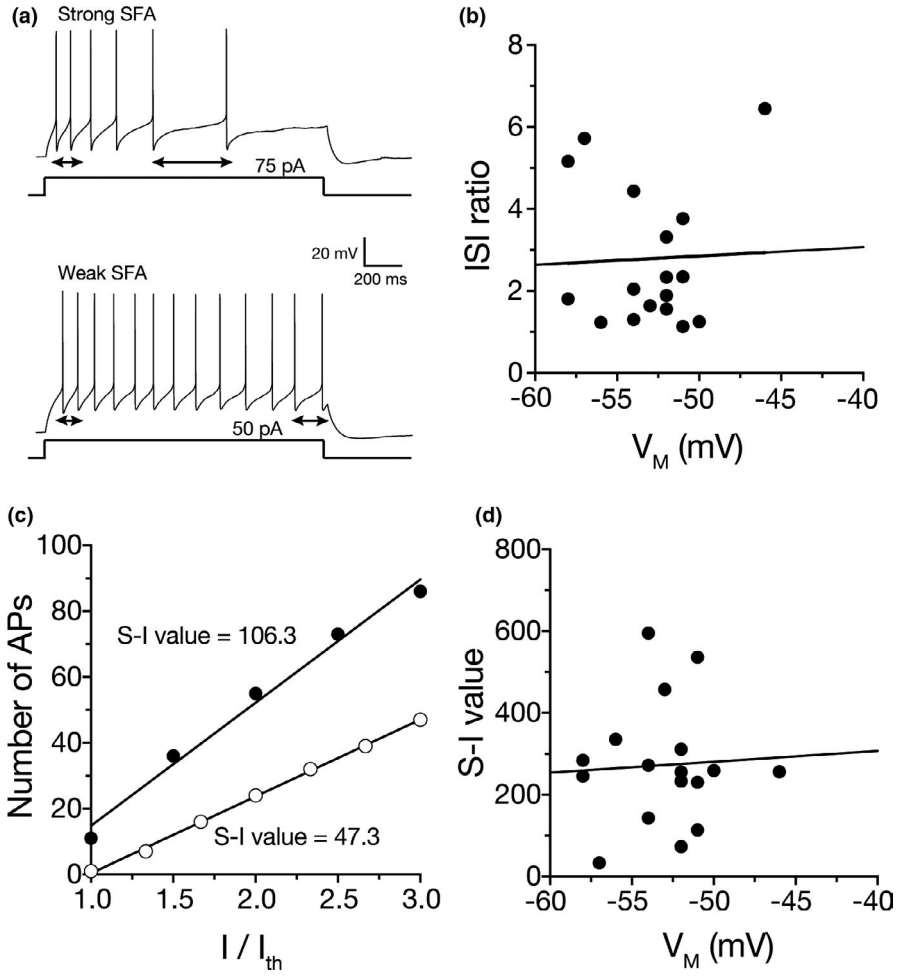

FIGURE 1 Spike frequency adapatation varies among statum orienst interneurons. (a) Voltage traces from weak SFA and strong SFA cells showing the smallest current step to elicit action potentials. Note the strong spike frequency adaptation in the strong SFA cell. Cells were held at −70 mV. (b) The ISI ratio does not have a significant relationship to the resting membrane potential (SFA range across all cells: 1.1–6.5; Pearson's $r = -0.0015$, $p = 0.88$). ISI ratio was determined by dividing the ISI between the last to spikes (arrow 1) by the ISI of the first two spikes (arrow two). (c) Number of action potentials as a function of normalized current injected. The area under the curve (S-I value) indicates the strength of adaptation. (d) S-I value is not correlated with VM (mV)

3.2 | Relationship of physiological parameters to spike frequency adaptation

The subthreshold properties of hippocampal interneurons, including input resistance (R_N) and voltage sag (max R_N/steady-state R_N), can vary widely across the many interneuron types (for review see Pelkey et al. (2017)). We measured neuronal input resistance (both maximum and steady state), voltage sag, and rebound and plotted each as a function of SFA (ISI ratio). All four subthreshold parameters were correlated with cell SFA. Maximum R_N (Pearson's $r = -0.6047$, $p = 0.0078$) and steady-state R_N (Pearson's $r = -0.6621$, $p = 0.0028$) were negatively correlated with ISI ratio (Figure 2a–c). Voltage sag (Pearson's $r = 0.7822$, $p = 0.0002$) and rebound slope (Pearson's $r = -0.8941$, $p < 0.0001$) were positively correlated with ISI ratio (Figure 2d–f; note the negative r value for rebound is because greater rebound is a more negative slope). Like subthreshold properties, action potential properties can vary widely across hippocampal interneurons (for review see Pelkey et al. (2017)). Unlike subthreshold properties, however, there was no correlation between action potential threshold (Pearson's $r = 0.2555$; $p = 0.3223$), action potential half-width (Pearson's $r = 0.1201$; $p = 0.6462$), action potential maximum dV/dt (Pearson's $r = -0.0637$; $p = 0.8081$), or minimum dV/dt (Pearson's $r = 0.1396$; $p = 0.5931$) (Figure 2g–l).

3.3 | Clustering of heterogeneous SFA interneurons

We used these physiological parameters and a k-means clustering algorithm to investigate whether the stratum oriens interneurons we recorded could be separated into functionally distinct categories (Table 1; Figure 3a). First, we determined the optimal number of clusters given our data set. Our analyses in NbClust in R (Charrad et al., 2014) revealed two clusters were optimal ($k = 2$, Figure 3b). Our data set neatly partitioned into two distinct clusters based off of these physiological characteristics (Figure 3c–e). Given the large sag and rebound, consistent with the hyperpolarization activated current I_h, and strong SFA associated with cluster 2, we will tentatively refer to these cells as Low Threshold High I_h (LTH) interneurons and refer to cells in cluster 1 as canonical OLM interneurons. We observed OLM (weak SFA) and LTH (strong SFA) neurons with roughly equal probabilities, indicating LTH cells may not be simply a small population of SO interneurons (OLM 10/18 cells, LTH 8/18 cells). Based on the two clusters produced by k-means clustering, we compared the action potential and subthreshold properties between these two groups.

3.4 | Active properties

The results of our clustering analysis suggest our recordings from stratum oriens interneurons can be divided into at least two groups based on physiological characteristics. We next asked if the two groups produced by k-means clustering had different intrinsic properties. We observed marked differences in SFA (measured as the ISI ratio) between OLM and LTH cells. SFA can be used as a pivotal parameter to differentiate inhibitory interneuron subtypes (reviewed in Pelkey et al. (2017)). In the literature, fast spiking interneurons are known to be non-adapting with little change in ISI ratio across spike trains. OLM cells and CCK basket cells exhibit adapting phenotypes with varied changes in their ISI ratio across a range of action potentials. In contrast, a group of interneuron selective interneurons exhibit a unique "stuttering" spiking behavior where they spike in high frequency clusters of spikes followed by a silence of activity (Hu et al., 2014; Pelkey et al., 2017; Tricoire et al., 2011). We measured action potential firing across a range of depolarizing current injection amplitudes. We found that OLM cells fire significantly more action potentials compared to LTH cells (Figure 4a and b; repeated measures ANOVA, main effect of cell type (F (9, 144) = 279.3; $p = 0.0023$)). We isolated the first action potential elicited by the smallest current injection for analysis (Figure 4c and d). Consistent with our observations in Figure 2, there was no significant difference in action potential threshold, half-width, min or max dV/dt between OLM and LTH cells (Figure 4e–h). These data suggest that the sodium and potassium conductances that contribute to the first action potential were not significantly different between OLM and LTH cells.

3.5 | Passive properties

There was no difference in resting membrane potential between OLM and LTH cells (Figure 1b). In agreement with previous reports on stratum oriens interneurons, both OLM and LTH cells had resting membrane potentials more depolarized compared to hippocampal pyramidal cells (Maccaferri & McBain, 1996; Tricoire et al., 2011). OLM cells have significantly higher input resistance (R_N) compared to LTH cells (Figure 5b). OLM neurons express h-channels, which is made evident by small voltage sag during the onset and rebound during the offset of hyperpolarizing current injections (Lupica et al., 2001; Maccaferri & McBain, 1996; Zemankovics et al., 2010). We measured sag as the difference between the maximum voltage and steady state as indicated by the arrows. (Figure 5c; grey indicates LTH cells and black indicates OLM cells). While both OLM and LTH cells display sag and rebound, both the sag and rebound were significantly larger in LTH cells compared to OLM cells (Figure 5d–f).

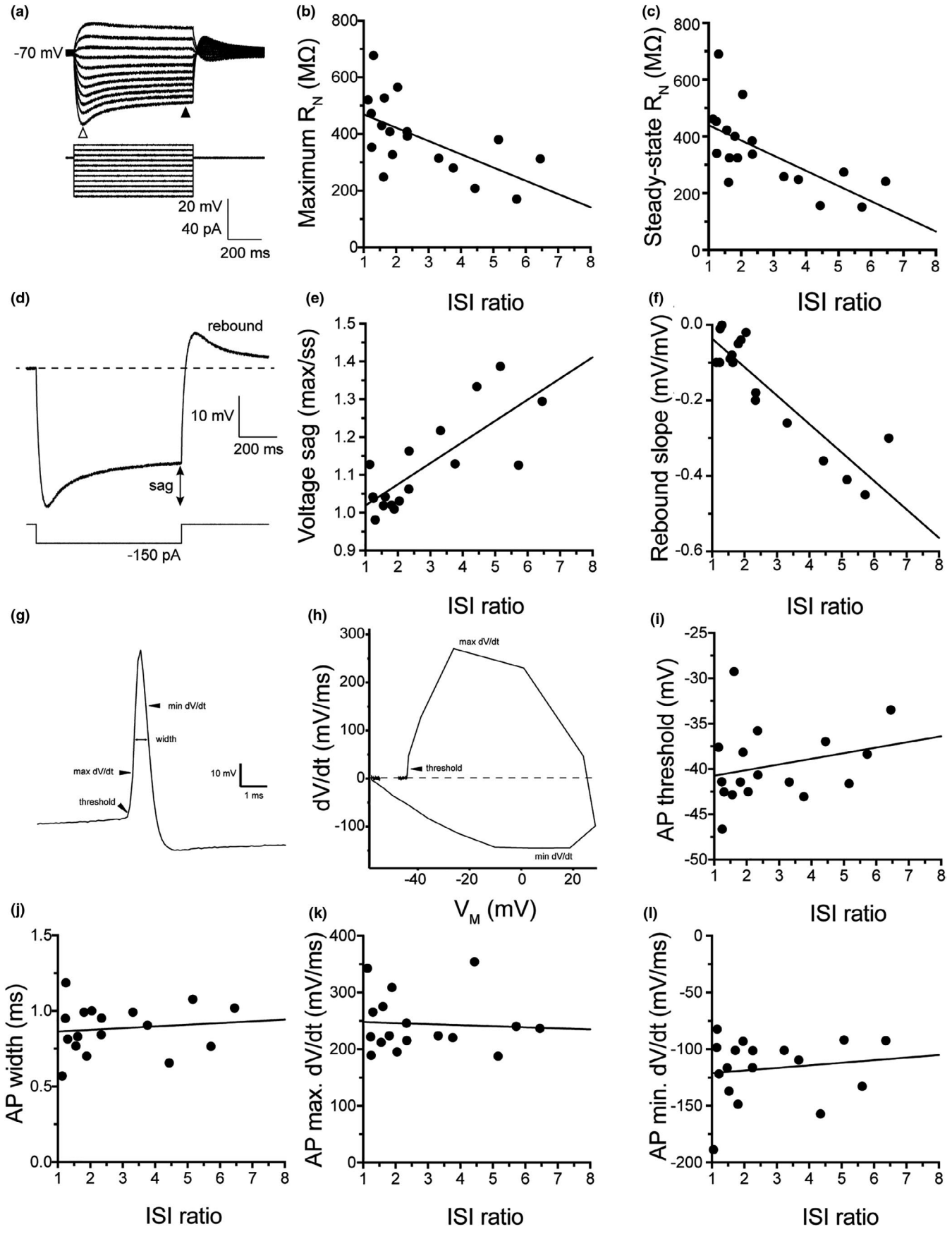
(a)
-70 mV
20 mV
40 pA
200 ms
(b)
Maximum R_N (MΩ)
ISI ratio
(c)
Steady-state R_N (MΩ)
ISI ratio
(d)
rebound
10 mV
200 ms
sag
-150 pA
(e)
Voltage sag (max/ss)
ISI ratio
(f)
Rebound slope (mV/mV)
ISI ratio
(g)
min dV/dt
width
max dV/dt
threshold
10 mV
1 ms
(h)
max dV/dt
threshold
min dV/dt
dV/dt (mV/ms)
V_M (mV)
(i)
AP threshold (mV)
ISI ratio
(j)
AP width (ms)
ISI ratio
(k)
AP max. dV/dt (mV/ms)
ISI ratio
(l)
AP min. dV/dt (mV/ms)
ISI ratio

FIGURE 2 Relationship of physiological parameters to ISI ratio. (a) Example voltage traces indicating the measurements of maximum (open arrow) and steady state voltages (closed arrow) were taken. (b–c) There is a strong correlation of steady state and maximum input resistance with the ISI ratio (Maximum R_N [Pearson's $r = -0.6047$, $p = 0.0078$] and steady-state R_N [Pearson's $r = -0.6621$, $p = 0.0028$]). (d) example voltage traces of the voltage sag and rebound response. (e–f) There is a strong relationship between the ISI ratio with voltage sag and rebound (Voltage sag [Pearson's $r = 0.7822$, $p = 0.0002$] and rebound slope [Pearson's $r = -0.8941$, $p < 0.0001$]). (g) Example voltage trace of a single AP with arrows indicating where different properties are measured. (h) Example phase plane plot of a single AP. Note where maximum dV/dt, minimum dV/dt, and AP threshold are indicated. (i–l) Active properties measured from the first action potential. There is no relationship between AP threshold (Pearson's $r = 0.2555$; $p = 0.3223$), half-width (Pearson's $r = 0.1201$; $p = 0.6462$), maximum dV/dt (Pearson's $r = -0.0637$; $p = 0.8081$), or minimum dV/dt (Pearson's $r = 0.1396$; $p = 0.5931$)

TABLE 1 Table of the parameters used in the k-means clustering algorithm from Figure 3

K Means Chart	RMP (mV)	Rebound	ISI Ratio	Sag	R_N SS	R_N Max	Max Firing
LTH	−54 ± 1.35	−0.32 ± 0.04	4.16 ± 0.02	1.22 ± 0.03	295 ± 23.47	360 ± 28.06	43 ± 3.52
OLM	−52 ± 0.97	−0.04 ± 0.01	1.58 ± 0.03	1.03 ± 0.01	469 ± 31.21	487 ± 32.13	63 ± 4.51

The analysis used the resting membrane potential (RMP, mV), rebound (mV/mV), ISI ratio (first ISI/last ISI), sag (R_N SS/R_N Max), steady-state input resistance (R_N SS, Mega Ohm), maximum input resistance (R_N Max, Mega Ohm), and max firing rate (Hz).

3.6 | OLM and LTH cells express SST

The use of transgenic mouse lines to target interneuron subtypes has been critical to furthering the study of physiological properties of different interneurons (Taniguchi et al., 2011). We recorded fluorescent cells from somatostatin:cre Ai14 mice (SST:cre Ai14) to determine if OLM and LTH cells could both be found in the fluorescent cell population, indicating the expression of somatostatin. We recorded from 13 fluorescent cells (representative images Figure 6b and d), post hoc analysis of subthreshold and SFA properties indicated 7/13 cells were LTH cells and 6/13 cells were OLM cells. All LTH cells exhibited strong SFA, sag, and rebound properties (Figure 6a) and had oblong cell bodies in the stratum oriens (Figure 6b). OLM cells exhibited weak SFA spiking profile with moderate sag (Figure 6c). Our results suggest the use of SST:cre Ai14 mouse lines indeed lead to sampling a heterogeneous population of interneuron subtypes (also indicated in (Hu et al., 2013)), particularly in the stratum oriens where both OLM and LTH cells were found in this mouse model.

3.7 | OLM and LTH cells have similar neuronal morphology

The properties of hippocampal pyramidal neurons vary along the dorsal ventral axis of the hippocampus (Dougherty et al., 2012; Kim & Johnston, 2015; Malik et al., 2016; Ordemann et al., 2019). More recently, OLM cells were shown to have distinct intrinsic physiological properties depending on the dorsal ventral location of the cell (Hilscher et al., 2019). To determine if the dorsal ventral location of our recordings biased our findings, we mapped our slices to examine their dorsal ventral position within the hippocampus (Malik et al., 2016). Our analysis confirms that our recordings were made from slices taken from the middle hippocampus and that there was no significant difference in the dorsal ventral location of our OLM and LTH cell recordings (Figure 7a and c). We analyzed the position of our recovered and reconstructed neurons and observed no difference in where OLM and LTH cells are found in the subbicular-CA3 axis of the hippocampus (Figure 7b). Differences in neuronal morphology will strongly influence physiology. Recorded cells were filled with neurobiotin and reconstructed (Figure 7d). We did not observe gross differences in the somato-dendritic morphological structure of OLM and LTH cells (Figure 7e). Both cells had oblong cell bodies in the stratum oriens with dendrites extending along the CA3–subicular axis. A few LTH cells did seem to have dendrites that extended into the pyramidal layer (2 of 6 reconstructions). Axons recovered from OLM cells showed typical extensive branching in the SLM (2 of 5 reconstructions) while axons recovered from LTH cells seemed to also descend out of the pyramidal layer. (2 of 6 reconstructions).

3.8 | Higher I_h density in LTH cells

Our current-clamp recordings showed that OLM cells have higher R_N and smaller sag and rebound compared to LTH cells. OLM cells, like CA1 pyramidal neurons, express hyperpolarization activated non-selective cation channels (I_h; (Halliwell & Adams, 1982; Lupica et al., 2001; Maccaferri & McBain, 1996; Matt et al., 2011)). Based on the larger sag and rebound, we hypothesized that LTH cells had higher I_h compared to OLM cells. We used a combined current-clamp/voltage-clamp approach to measure the density of I_h in OLM and LTH cells (Figure 8a). After we used depolarizing

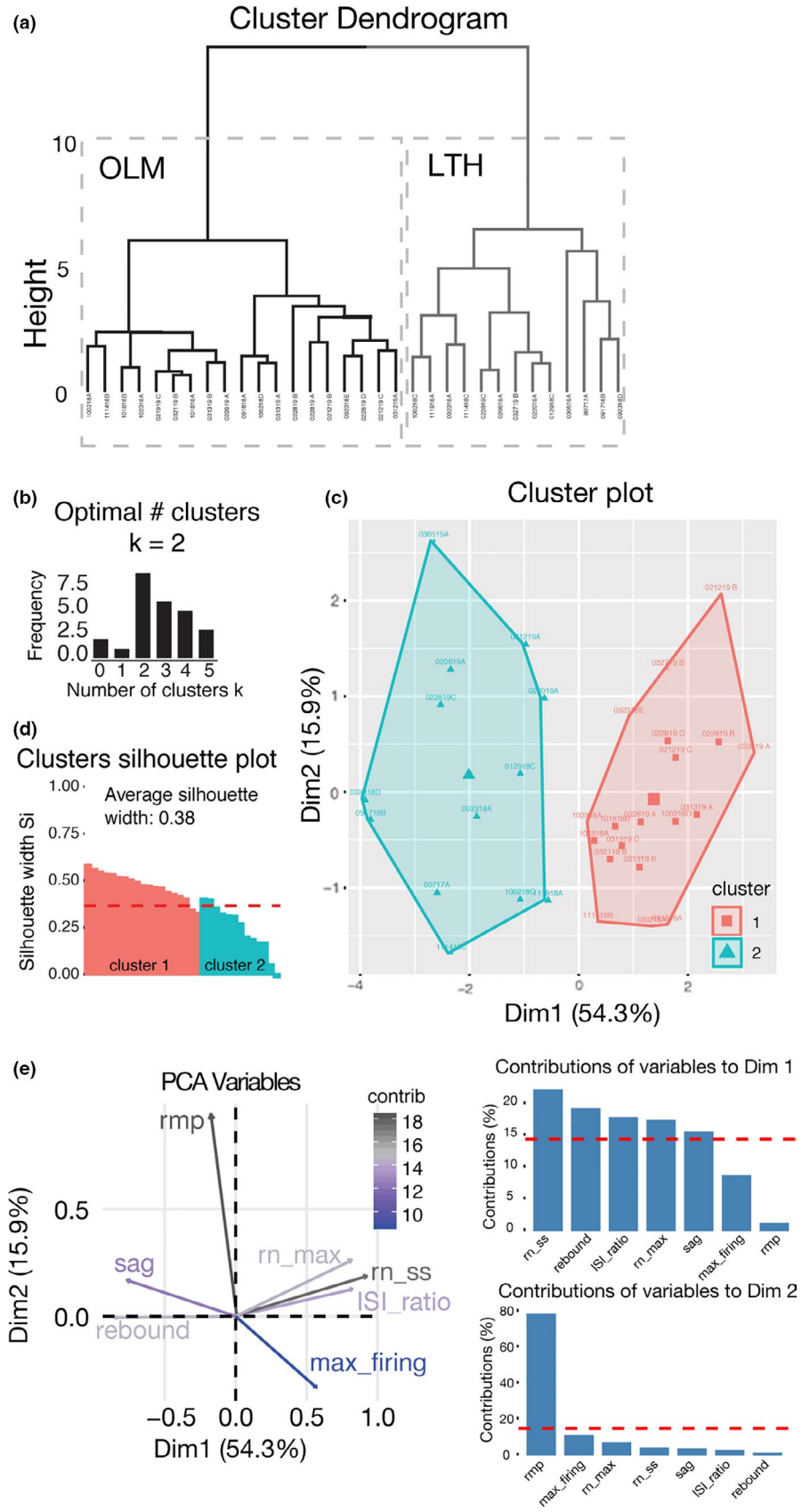

FIGURE 3 OLM and LTH cells separate into clusters based on intrinsic physiology. (a) Cluster dendrogram of OLM and LTH cell clusters based on intrinsic electrophysiological properties. (b) The optimal number of clusters indicated by NbClust in R Statistics, the optimal number of clusters for our data set $k = 2$. (c) Cluster plot of principal component analysis (PCA) dimensions cluster 1 cells are LTH cells and cluster 2 cells are OLM cells. (d) Silhouette plot of clusters 1 and 2. The average silhouette width was 0.38. (e) Vector plot of PCA variables and their percent contribution to the clustering of OLM and LTH cells. Bar graphs show the contribution of variability to the two dimensions that carry a majority of the variability of the data set. Bars above the red line indicate variables that contribute more than the calculated average variability of any given parameter

current injections to evoke action potential firing to measure ISI ratio, we switched to voltage clamp and bath applied 1 μM TTX to block voltage-gated Na^+ channels; 10 mM TEA, 5 mM 4-AP and 200 μM $BaCl_2$ to block voltage-gated K^+ channels; and 100 μM $CdCl_2$ to block voltage-gated calcium channels. In order to compare to previously published

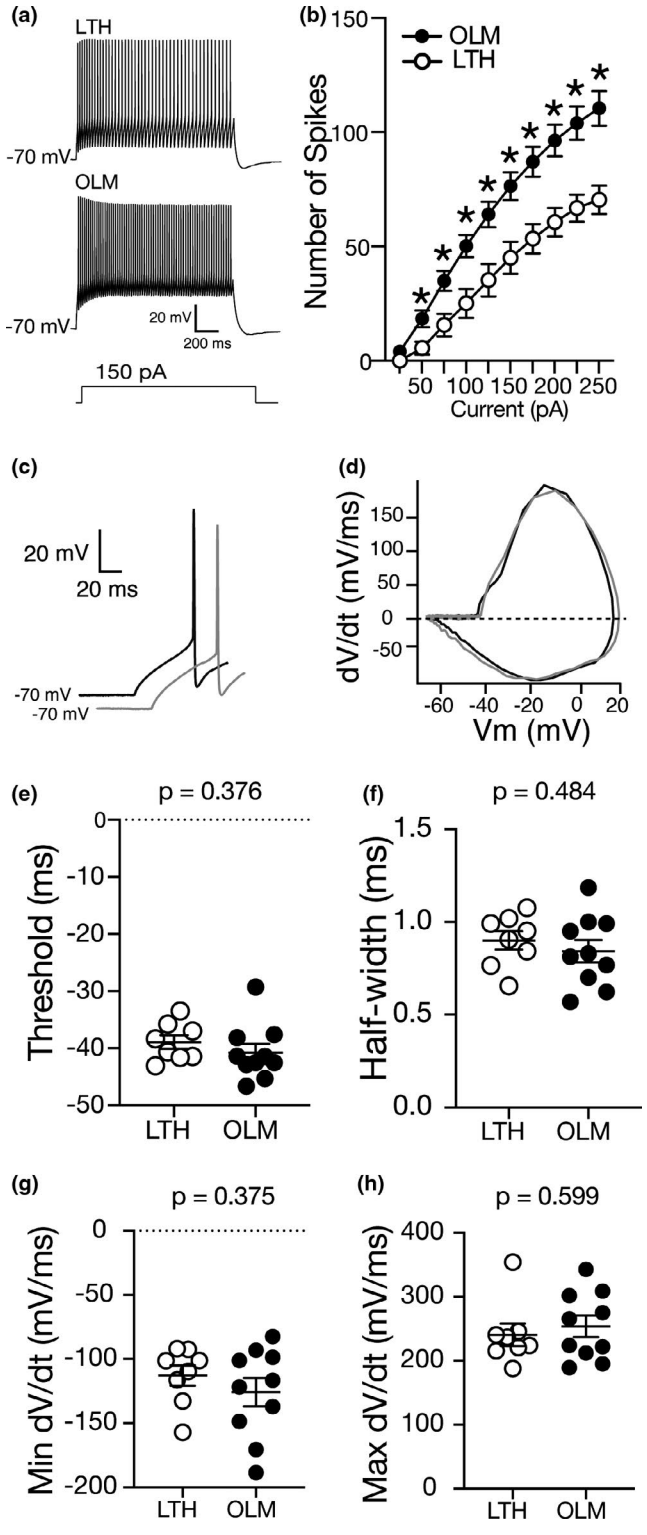

FIGURE 4 OLM have higher firing rates than LTH cells. (a) Voltage traces showing action potential firing from an LTH and OLM cells in response to a 1.5 s, 150 pA current injection. (b) Summary plot showing that OLM cells fire significantly more action potentials compared to LTH cells across a range of current injection amplitudes (repeated measures ANOVA, main effect of current (F (9, 144) =279.3; p = 0.0001), main effect of cell type (F (1, 16) =13.12; p =.0023), interaction between cell type and current (F (9, 44) =9.66; p = 0.0001). (c) First AP on which analysis was conducted in LTH (grey) and OLM (black) neurons. (d) Phase plane plot of the first spike in LTH (grey) and OLM (black) neurons. (e–h) Action potential threshold (e), half-width (f), minimum dV/dt (g) and maximum dV/dt (h) are not significantly different between LTH and OLM cells

results, we used the same whole-cell voltage clamp approach described in Maccaferri & McBain, 1996. We used a series of hyperpolarizing voltage steps to elicit a slowly activating inward current (Figure 8b and c). The density of I_h was significantly higher in LTH cells compared to OLM cells (Figure 8d and e, black circles). The current was completely blocked by the h-channel blocker ZD7288 (50 μM) (Figure 8d and e, grey circles). These results suggest that the subthreshold differences between OLM and LTH cells were due in part to the differential expression of the hyperpolarization activated current I_h.

4 | DISCUSSION

Interneurons exhibit a wide range of physiological and molecular profiles leading many researchers to question what defines a specific interneuron subtype. Here we use a combination of physiological, morphological, and biochemical approaches to identify a previously uncharacterized subtype of hippocampal stratum oriens interneuron, LTH cells. We identified a number of different intrinsic physiological properties between OLM and LTH cells. LTH cells fire fewer action potentials in response to depolarizing current steps when compared to OLM cells. Single action potential analysis revealed no differences in threshold, amplitude, half-width, or min/max dV/dt, which suggests that the ion channel conductances underlying these properties may not be significantly different between LTH and OLM cells. We found that the input resistance of LTH was significantly lower compared to OLM cells. While the decrease in firing may be related to the lower input resistance of LTH cells, our analysis does not capture how the spike waveform changes with concurrent spikes across the current step, which may reveal an underlying conductance that increases the adaptation of LTH cells leading to a decrease in spikes. Voltage sag was steeper and rebound larger in LTH cells compared to OLM cells. Sag and rebound are current clamp indicators of h-channel function leading us to hypothesize that LTH cells have higher h-channel current compared to OLM neurons. Indeed, we found that I_h density is significantly higher in LTH cells compared to OLM cells.

4.1 | Ion channel contributions to LTH neuron intrinsic properties

These intrinsic properties of neurons shape the integration of synaptic inputs, precision of action potential output, and

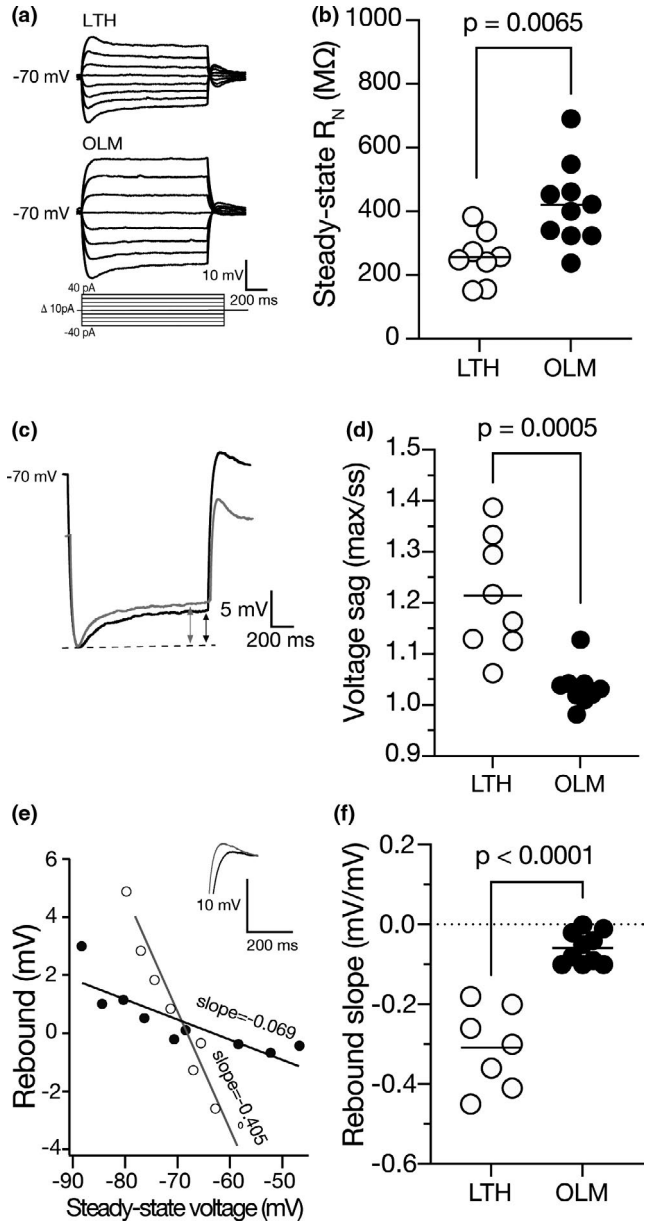

FIGURE 5 LTH cells have lower input resistance compared to OLM cells. (a) Voltage responses to a family of subthreshold current injections from OLM and LTH cells. (b) OLM cells have a significantly higher input resistance (R_N) than LTH cells (unpaired *t*-test, $p = 0.006$). (c) Voltage traces indicating the sag in LTH (grey) and OLM (black) cells. The arrows indicate the maximum voltage and the steady state of the cell. D. LTH cells have significantly higher sag compared to OLM cells (unpaired *t*-test, $p < 0.001$). (e) Measurement of rebound in the traces seen in C and indicated by the traces of LTH (grey) and OLM (black) cell voltage traces of rebound. (f) LTH cells have significantly more rebound than OLM cells (unpaired *t*-test, $p < 0.001$)

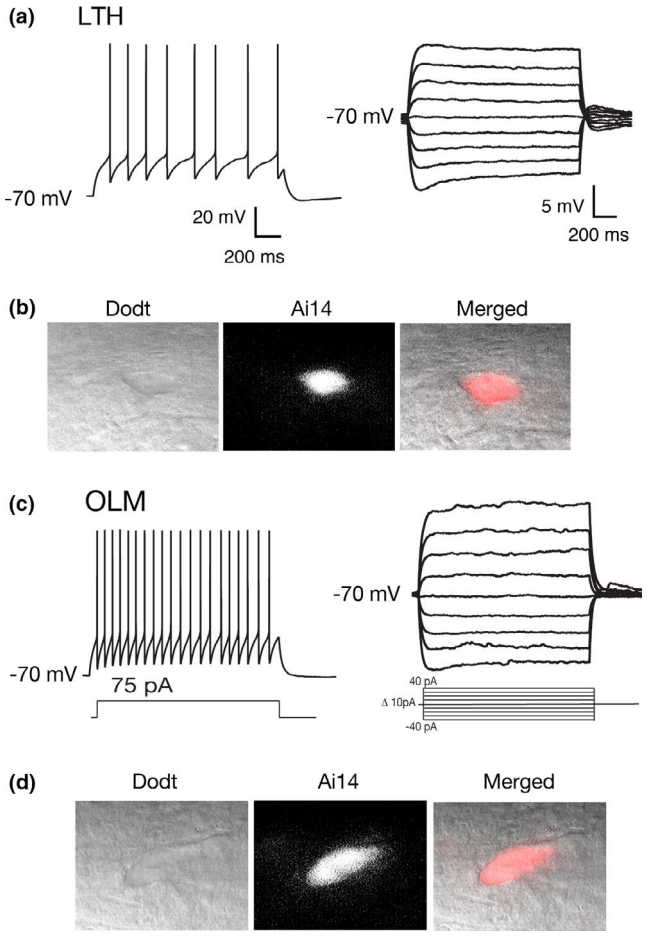

FIGURE 6 LTH and OLM cells are found in SST:cre Ai14 mice. (a) representative firing and subthreshold traces of an Ai14+ LTH neuron recording. ($n = 7/13$ recorded cells). (b) LTH interneuron under Dodt contrast, expressing Ai14 driven florescence, and both images overlayed. (c) representative firing and subthreshold traces for an Ai14+ OLM neuron recording. ($n = 8/13$ recorded cells). (d) OLM neuron under Dodt contrast, expressing Ai14, and both images overlayed

contribution to the local circuitry. Our data show LTH cells have significantly higher density of I_h resulting in altered subthreshold properties (R_N, sag, and rebound). Differences in I_h between OLM and LTH cells suggest key differences in the ability of LTH neurons to integrate synaptic activity and trigger action potential output. The lower input resistance of LTH cells suggests that larger synaptic currents would be required to fire action potentials. In addition, the higher density of h-channels would also limit the summation of synaptic inputs. Taken together, this suggests that both magnitude and temporal frequency of synaptic inputs would need to be higher to drive LTH cells to fire action potentials compared to OLM cells.

The higher density of I_h would be expected to lower input resistance and depolarize the resting membrane potential (Lupica et al., 2001). While we did find that the input resistance of LTH cells was lower compared to OLM cells, there was no difference in resting membrane potential. This could indicate that there is not as much I_h at rest in LTH cells or there are likely additional channels active at or near the resting membrane potential may be different between LTH and OLM cells. LTH cells exhibit stronger SFA compared

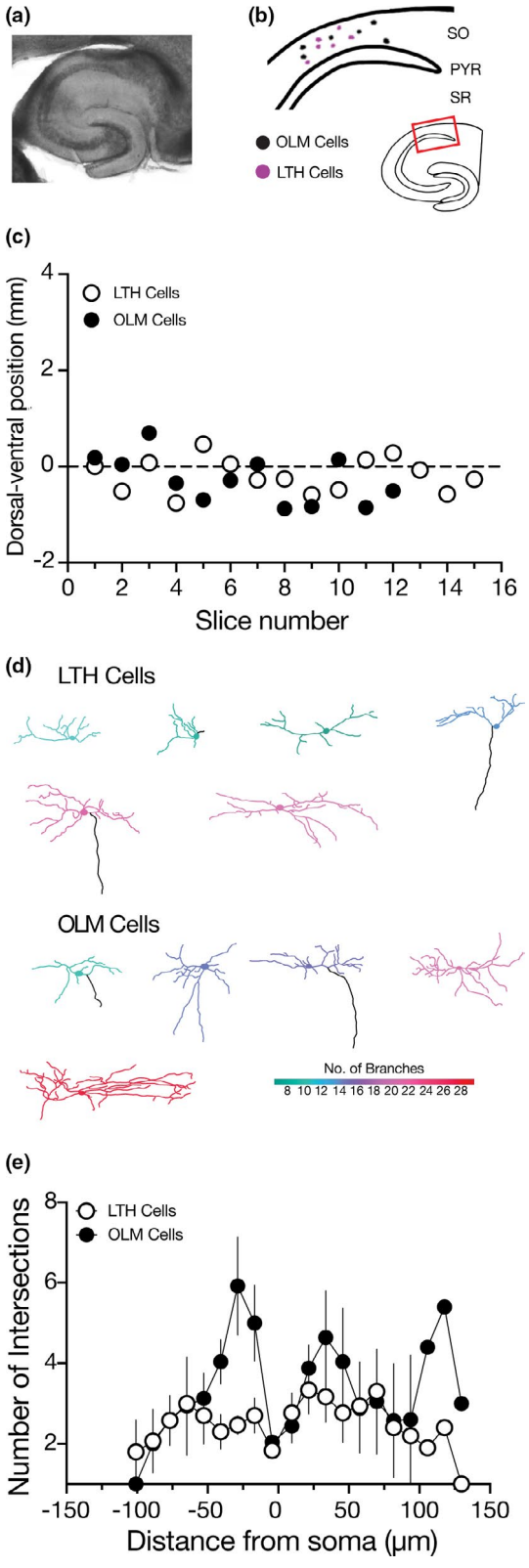

FIGURE 7 Dorsal/ventral position is not different between LTH and OLM cells, morphology. (a) bright field image at 5× showing the CA1 area of the hippocampus. (b) schematic of the location of fully recovered and reconstructed LTH and OLM cells recordings in the CA1 SO. Black indicates OLM cell body and pink indicates LTH cell body. (c) Dorsal/ventral position of LTH and OLM cells from all slices used in experiments. (d) Neuronal reconstructions of LTH and OLM cells. Black lines indicate the axon. The color coding indicates the number of branch points using the scale in the lower right corner. (e) Scholl analysis of morphological constructions of LTH and OLM

to OLM cells. It is not likely differences in I_h density account for the SFA, due to h-channels not being active during large depolarizations. Several different potassium channels can contribute to SFA including Ca^{2+}-activated BK and SK channels, and m-channels (Gu et al., 2005, 2007; Peters et al., 2005). Further study is required to determine if there are differences in the expression and or function of these channels between LTH and OLM cells.

4.2 | LTH interneuron identity

Given the vast diversity of hippocampal interneurons, it is not surprising to find subtypes of interneurons that lack characterization. A previous study dissected different interneuron types based on developmental lineage and uncovered many uncharacterized interneurons (Tricoire et al., 2011). Recent momentous undertakings have revealed that many cell types still lack proper descriptions (Gouwens et al., 2020; Harris et al., 2018). LTH cells appear to be one of these interneuron subtypes that have not been thoroughly characterized. Trilaminar and back propagating interneurons are also found in CA1 SO and present with oblong cells bodies with dendrites that extend perpendicular to pyramidal CA1 neurons (Sik et al., 1994, 1995). It is unlikely that LTH cells are trilaminar cells considering trilaminar cells do not express a sag and rebound response (Gloveli et al., 2005). Back propagating interneurons are typically found in the alveus of CA1, but can also been seen in CA1 SO. These particular interneurons have an axon that extends into CA3. The morphological analysis of the LTH cells in our study did not seem to have any axon processes in CA3, however, this could be due to an incomplete fill of the axon or the axon not being planar in our slice preparation. A paper from Zemankovics et al., 2010 grouped together cells in the CA1 SO that seemed to be projecting neurons with similar physiological properties and diverse morphological properties (OR group). This group of cells exhibits a steeper sag and rebound response to depolarize steps when compared to OLM cells. However, whole cell voltage clamp study of I_h in OR and OLM neurons did not reveal any significant differences (Zemankovics et al., 2010). This could be due to the OR group of neurons being heterogeneous indicating LTH cells could potentially be a part of the neurons recorded in the OR group. LTH neurons have very likely been recorded from and included in many studies, here we present a detailed characterization of the intrinsic properties of LTH cells to create a foundation for understanding how these neurons may impact hippocampal circuitry.

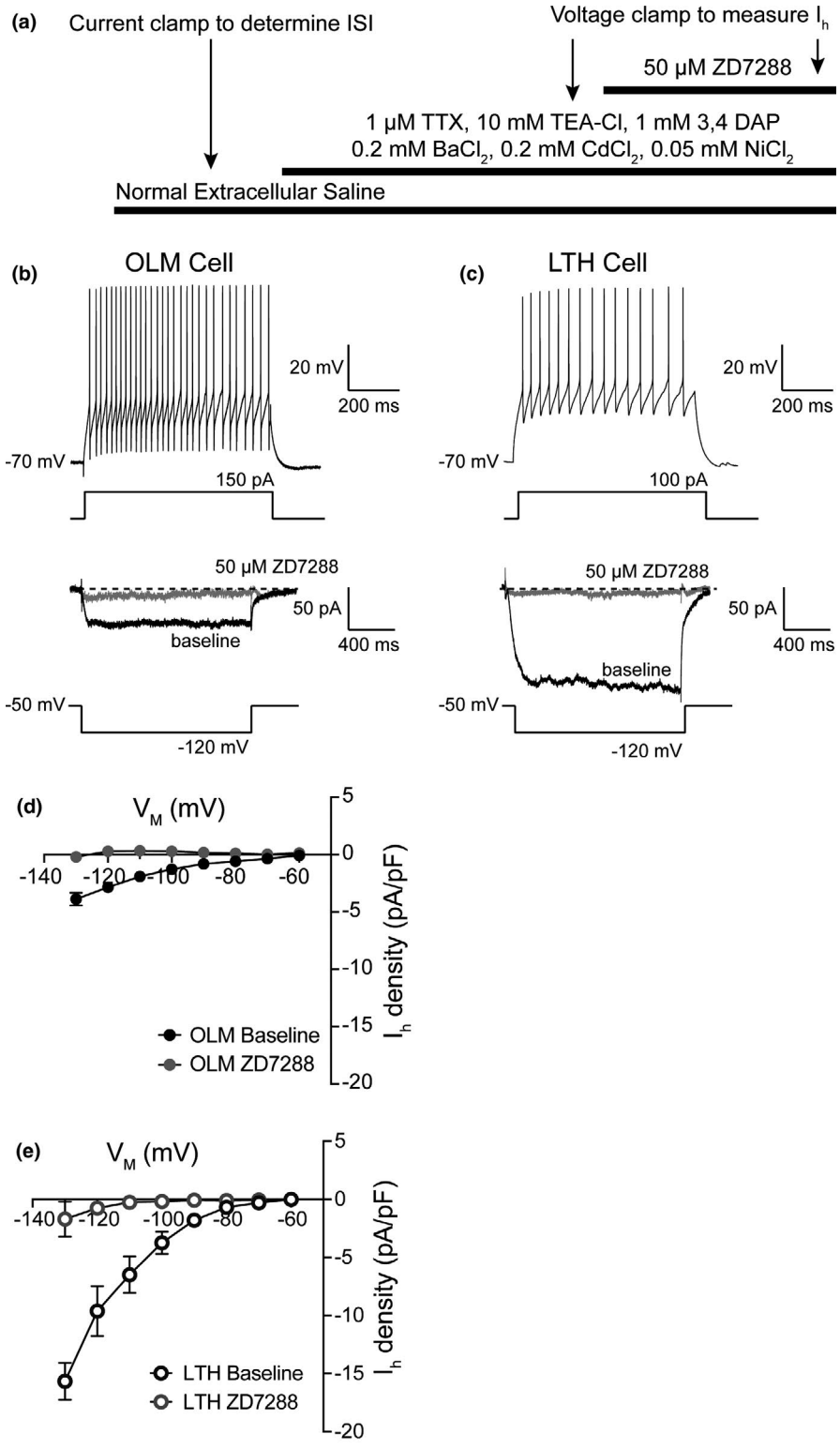

FIGURE 8 I_h density is higher in LTH cells. (a) Experimental design for measuring I_h from OLM and LTH cells. (b) Representative OLM cell showing action potential firing with high ISI ratio measured in current clamp (top) and I_h measured in voltage clamp (bottom). (c) Representative LTH cell showing action potential firing with low ISI ratio measured in current clamp (top) and I_h measured in voltage clamp (bottom). (d) I_h density before and after application of 50 µM ZD7288 in OLM cells. (e) I_h density measured before and after application of 50 µM ZD7288in LTH cells

4.3 | Contrasting LTH and OLM interneurons

It is likely the case, as in many biological systems, that interneuron subtypes cannot be split into discrete subtypes, but instead exist on an axis of properties that define their role in information processing. While many interneuron subtypes do exist on graded axes of properties, given our current data, it seems unlikely for LTH cells to be a subset of the OLM interneurons. While the OLM cells typically originate from the medial ganglionic eminence, a subtype of OLM cells originate from the central ganglionic eminence (Chittajallu et al., 2013; Winterer et al., 2019). These two subclasses of OLM cells are indistinguishable based on physiology. In contrast, we found

marked differences in both the firing patterns and subthreshold physiological properties between LTH and OLM cells. OLM interneuron properties can vary based on the dorsal/ventral location of the cell. Ventral OLM cells exhibit more adapting firing rates compared to dorsal cells. Dorsal OLM cells also show a steeper sag response compared to ventral interneurons (Hilscher et al., 2019). We show that both LTH and OLM cells are found in the same dorsal/ventral extent within the middle region of the hippocampus. We further demonstrate a separation of LTH cells from OLM cells based on sampled physiological properties with a k-means clustering algorithm. Taken together, we suggest that LTH cells are a separate class of stratum oriens interneuron.

4.4 | Somatostatin expression and morphology of LTH interneurons

While biochemical markers such as parvalbumin (PV) and somatostatin (SST) are traditionally used to differentiate subtypes of hippocampal interneurons, many cells express both PV and SST or other combinations of common inhibitory interneuron markers (Losonczy et al., 2002; Maccaferri et al., 2000; Tricoire et al., 2011). We observed both LTH and OLM interneurons in SST:cre Ai14 leading us to believe LTH cells express SST. Action potential firing is also used to separate classes of interneurons as "fast spiking" versus "regular spiking." Some interneuron classes have distinctive dendritic and axonal arbors but the number of interneurons that can identified by morphology alone, particularly in under characterized interneurons, is limited (Ascoli et al., 2008; DeFelipe et al., 2013; Maccaferri & Lacaille, 2003). LTH cells may have an axon that is not planar in our current slice preparation, indeed it would be interesting to investigate the full extent of LTH neuron morphology, particularly the axon, using modern tracing methods. It has become increasingly common to determine the genetic profile of inhibitory interneurons as well, we have gained many insights from recent literature exploring an array of genetic markers of interneuron subtypes that have recorded physiological and reconstructed morphological properties (as in Gouwens et al., 2020). Large strides in genetic and big data techniques have allowed scientists to study inhibitory interneurons in exquisite detail. Genetic mouse models and intersectional genetics have made targeted approaches accessible to begin untangling interneuron subtypes functional role in circuits. While we do not show the full molecular profile of LTH cells here, it will be interesting to determine if additional key interneuron markers, if any, are expressed. It is the constellation of properties exhibited by a neuron that determines its function in a circuit. While the cell body and dendrites of LTH neurons reside within stratum oriens, their role in the hippocampal circuit remains unknown. Future studies using targeted, paired recordings between LTH neurons and CA1 pyramidal neurons will provide critical information related to the role LTH neurons may play in hippocampal information processing. Taking all of these properties into account may be necessary to describe how OLM and LTH cells are both different and related to each other.

ACKNOWLEDGMENTS

We thank Dr. Chris McBain for generously providing protocols for slice processing for reconstructions, assistance with the k-means clustering code, and helpful discussion on this manuscript, Jarod Tolbert for conducting the dorsal ventral analysis on processed slices, Dr. Richard Gray for assistance with analysis programs, Meagan Volquardsen for genotyping and mouse colony management, members of the Johnston lab for helpful comments and lively discussion on this manuscript, and to Emily Aster Jones and Jessica Chancey for helpful review of our manuscript.

CONFLICT OF INTEREST

The authors declare no conflicts of interest.

AUTHOR CONTRIBUTIONS

L.T.H. and D.H.B. designed the experiments; L.T.H., G.J.O, and D.H.B. acquired the data; L.T.H., G.J.O, and D.H.B. analyzed the data; L.T.H. and D.H.B. interpreted results of the experiments; L.T.H. and D.H.B. prepared the figures; L.T.H. and D.H.B. drafted the manuscript; L.T.H., G.J.O., and D.H.B. edited and revised the manuscript.

ORCID

Lauren T. Hewitt https://orcid.org/0000-0001-7270-7679

REFERENCES

Arshadi, C., Günther, U., Eddison, M., Harrington, K. I. S., & Ferreira, T. A. (2021). SNT: A unifying toolbox for quantification of neuronal anatomy. *Nature Methods*, *18*, 374–377. https://doi.org/10.1038/s41592-021-01105-7.

Ascoli, G. A., Alonso-Nanclares, L., Anderson, S. A., Barrionuevo, G., Benavides-Piccione, R., Burkhalter, A., Buzsáki, G., Cauli, B., DeFelipe, J., Fairén, A., Feldmeyer, D., Fishell, G., Fregnac, Y., Freund, T. F., Gardner, D., Gardner, E. P., Goldberg, J. H., Helmstaedter, M., Hestrin, S., … The Petilla Interneuron Nomenclature Group (PING). (2008). Petilla terminology: Nomenclature of features of GABAergic interneurons of the cerebral cortex. *Nature Reviews Neuroscience*, *9*, 557–568.

Barkai, E., & Hasselmo, M. E. (1994). Modulation of the input/output function of rat piriform cortex pyramidal cells. *Journal of Neurophysiology*, *72*, 644–658. https://doi.org/10.1152/jn.1994.72.2.644

Bezaire, M. J., & Soltesz, I. (2013). Quantitative assessment of CA1 local circuits: Knowledge base for interneuron-pyramidal cell connectivity. *Hippocampus*, *23*, 751–785.

Blasco-Ibáñez, J. M., & Freund, T. F. (1995). Synaptic input of horizontal interneurons in stratum oriens of the hippocampal CA1

subfield: Structural basis of feed-back activation. *European Journal of Neuroscience*, *7*, 2170–2180.

Cadwell, C. R., Palasantza, A., Jiang, X., Berens, P., Deng, Q., Yilmaz, M., Reimer, J., Shen, S., Bethge, M., Tolias, K. F., Sandberg, R., & Tolias, A. S. (2016). Electrophysiological, transcriptomic and morphologic profiling of single neurons using Patch-seq. *Nature Biotechnology*, *34*, 199–203. https://doi.org/10.1038/nbt.3445

Charrad, M., Ghazzali, N., Boiteau, V., & Niknafs, A. (2014). NbClust: An R package for determining the relevant number of clusters in a data set. *Journal of Statistical Software*, *61*, 1–36.

Chittajallu, R., Craig, M. T., McFarland, A., Yuan, X., Gerfen, S., Tricoire, L., Erkkila, B., Barron, S. C., Lopez, C. M., Liang, B. J., Jeffries, B. W., Pelkey, K. A., & McBain, C. J. (2013). Dual origins of functionally distinct O-LM interneurons revealed by differential 5-HT_{3A}R expression. *Nature Neuroscience*, *16*, 1598–1607. https://doi.org/10.1038/nn.3538

Cobb, S. R., Buhl, E. H., Halasy, K., Paulsen, O., & Somogyi, P. (1995). Synchronization of neuronal activity in hippocampus by individual GABAergic interneurons. *Nature*, *378*, 75–78. https://doi.org/10.1038/378075a0

DeFelipe, J., López-Cruz, P. L., Benavides-Piccione, R., Bielza, C., Larrañaga, P., Anderson, S., Burkhalter, A., Cauli, B., Fairén, A., Feldmeyer, D., Fishell, G., Fitzpatrick, D., Freund, T. F., González-Burgos, G., Hestrin, S., Hill, S., Hof, P. R., Huang, J., Jones, E. G., … Ascoli, G. A. (2013). New insights into the classification and nomenclature of cortical GABAergic interneurons. *Nature Reviews Neuroscience*, *14*, 202–216. https://doi.org/10.1038/nrn3444

Dougherty, K. A., Islam, T., & Johnston, D. (2012). Intrinsic excitability of CA1 pyramidal neurones from the rat dorsal and ventral hippocampus. *Journal of Physiology*, *590*, 5707–5722. https://doi.org/10.1113/jphysiol.2012.242693

Freundl, T. F., & Buzsi, G. (1996). Interneurons of the hippocampus. *Hippocampus*, *6*, 347–470. https://doi.org/10.1002/(SICI)1098-1063(1996)6:4<347:AID-HIPO1>3.0.CO;2-I

Gloveli, T., Dugladze, T., Saha, S., Monyer, H., Heinemann, U., Traub, R. D., Whittington, M. A., & Buhl, E. H. (2005). Differential involvement of oriens/pyramidale interneurones in hippocampal network oscillations in vitro. *The Journal of Physiology*, *562*, 131–147.

Gouwens, N. W., Sorensen, S. A., Baftizadeh, F., Budzillo, A., Lee, B. R., Jarsky, T., Alfiler, L., Baker, K., Barkan, E., Berry, K., Bertagnolli, D., Bickley, K., Bomben, J., Braun, T., Brouner, K., Casper, T., Crichton, K., Daigle, T. L., Dalley, R., … Zeng, H. (2020). Integrated morphoelectric and transcriptomic classification of cortical GABAergic cells. *Cell*, *183*, 935–953.e19. https://doi.org/10.1016/j.cell.2020.09.057

Gu, N., Vervaeke, K., Hu, H., & Storm, J. F. (2005). Kv7/KCNQ/M and HCN/h, but not KCa2/SK channels, contribute to the somatic medium after-hyperpolarization and excitability control in CA1 hippocampal pyramidal cells. *Journal of Physiology*, *566*, 689–715.

Gu, N., Vervaeke, K., & Storm, J. F. (2007). BK potassium channels facilitate high-frequency firing and cause early spike frequency adaptation in rat CA1 hippocampal pyramidal cells. *The Journal of Physiology*, *580*, 859–882. https://doi.org/10.1113/jphysiol.2006.126367

Hájos, N., Pálhalmi, J., Mann, E. O., Németh, B., Paulsen, O., & Freund, T. F. (2004). Spike timing of distinct types of GABAergic interneuron during hippocampal gamma oscillations in vitro. *Journal of Neuroscience*, *24*, 9127–9137. https://doi.org/10.1523/JNEUROSCI.2113-04.2004

Halliwell, J. V., & Adams, P. R. (1982). Voltage-clamp analysis of muscarinic excitation in hippocampal neurons. *Brain Research*, *250*, 71–92. https://doi.org/10.1016/0006-8993(82)90954-4

Harris, K. D., Hochgerner, H., Skene, N. G., Magno, L., Katona, L., Gonzales, C. B., Somogyi, P., Kessaris, N., Linnarsson, S., & Hjerling-Leffler, J. (2018). Classes and continua of hippocampal CA1 inhibitory neurons revealed by single-cell transcriptomics. *PLOS Biology*, *16*, e2006387. https://doi.org/10.1371/journal.pbio.2006387

Hilscher, M. M., Nogueira, I., Mikulovic, S., Kullander, K., Leão, R. N., & Leão, K. E. (2019). Chrna2-OLM interneurons display different membrane properties and h-current magnitude depending on dorsoventral location. *Hippocampus*, *29*(12), 1224–1237.

Hu, H., Cavendish, J. Z., & Agmon, A. (2013). Not all that glitters is gold: Off-target recombination in the somatostatin–IRES-Cre mouse line labels a subset of fast-spiking interneurons. *Frontiers in Neural Circuits*, *7*, 1–4. https://doi.org/10.3389/fncir.2013.00195

Hu, H., Gan, J., & Jonas, P. (2014). Fast-spiking, parvalbumin+ GABAergic interneurons: From cellular design to microcircuit function. *Science*, *345*(6196), 1255263. https://doi.org/10.1126/science.1255263

Kim, C. S., & Johnston, D. (2015). A1 adenosine receptor-mediated GIRK channels contribute to the resting conductance of CA1 neurons in the dorsal hippocampus. *Journal of Neurophysiology*, *113*, 2511–2523. https://doi.org/10.1152/jn.00951.2014

Klausberger, T. (2009). GABAergic interneurons targeting dendrites of pyramidal cells in the CA1 area of the hippocampus. *European Journal of Neuroscience*, *30*, 947–957. https://doi.org/10.1111/j.1460-9568.2009.06913.x

Klausberger, T., & Somogyi, P. (2008). Neuronal diversity and temporal dynamics: The unity of hippocampal circuit operations. *Science*, *321*, 53–57.

Lacaille, J., Mueller, A., Kunkel, D., & Schwartzkroin, P. (1987). Local circuit interactions between oriens/alveus interneurons and CA1 pyramidal cells in hippocampal slices: Electrophysiology and morphology. *Journal of Neuroscience*, *7*, 1979–1993.

Lacaille, J. C., & Williams, S. (1990). Membrane properties of interneurons in stratum oriens-alveus of the CA1 region of rat hippocampus in vitro. *Neuroscience*, *36*, 349–359. https://doi.org/10.1016/0306-4522(90)90431-3

Lapray, D., Lasztoczi, B., Lagler, M., Viney, T. J., Katona, L., Valenti, O., Hartwich, K., Borhegyi, Z., Somogyi, P., & Klausberger, T. (2012). Behavior-dependent specialization of identified hippocampal interneurons. *Nature Neuroscience*, *15*, 1265–1271. https://doi.org/10.1038/nn.3176

Leão, R. N., Mikulovic, S., Leão, K. E., Munguba, H., Gezelius, H., Enjin, A., Patra, K., Eriksson, A., Loew, L. M., Tort, A. B. L., & Kullander, K. (2012). OLM interneurons differentially modulate CA3 and entorhinal inputs to hippocampal CA1 neurons. *Nature Neuroscience*, *15*, 1524–1530. https://doi.org/10.1038/nn.3235

Losonczy, A., Zhang, L., Shigemoto, R., Somogyi, P., & Nusser, Z. (2002). Cell type dependence and variability in the short-term plasticity of EPSCs in identified mouse hippocampal interneurones. *The Journal of Physiology*, *542*, 193–210. https://doi.org/10.1113/jphysiol.2002.020024

Lovett-Barron, M., Kaifosh, P., Kheirbek, M. A., Danielson, N., Zaremba, J. D., Reardon, T. R., Turi, G. F., Hen, R., Zemelman, B. V., & Losonczy, A. (2014). Dendritic Inhibition in the

Hippocampus Supports Fear Learning. *Science*, *343*, 857–863. https://doi.org/10.1126/science.1247485

Lupica, C. R., Bell, J. A., Hoffman, A. F., & Watson, P. L. (2001). Contribution of the hyperpolarization-activated current (I_h) to membrane potential and GABA release in hippocampal interneurons. *Journal of Neurophysiology*, *86*, 261–268.

Maccaferri, G. (2005). Stratum oriens horizontal interneurone diversity and hippocampal network dynamics. *The Journal of Physiology*, *562*, 73–80.

Maccaferri, G., David, J., Roberts, B., Szucs, P., Cottingham, C. A., & Somogyi, P. (2000). Cell surface domain specific postsynaptic currents evoked by identified GABAergic neurones in rat hippocampus in vitro. *The Journal of Physiology*, *524*, 91–116.

Maccaferri, G., & Lacaille, J.-C. (2003). Interneuron Diversity series: Hippocampal interneuron classifications–making things as simple as possible, not simpler. *Trends in Neurosciences*, *26*, 564–571.

Maccaferri, G., & McBain, C. J. (1995). Passive propagation of LTD to stratum oriens-alveus inhibitory neurons modulates the temporoammonic input to the hippocampal CA1 region. *Neuron*, *15*, 137–145. https://doi.org/10.1016/0896-6273(95)90071-3

Maccaferri, G., & McBain, C. J. (1996). The hyperpolarization-activated current (I_h) and its contribution to pacemaker activity in rat CAI hippocampal stratum oriens-alveus interneurones. *Journal of Physiology*, *12*.

Malik, R., Dougherty, K. A., Parikh, K., Byrne, C., & Johnston, D. (2016). Mapping the electrophysiological and morphological properties of CA1 pyramidal neurons along the longitudinal hippocampal axis. *Hippocampus*, *26*, 341–361. https://doi.org/10.1002/hipo.22526

Matt, L., Michalakis, S., Hofmann, F., Hammelmann, V., Ludwig, A., Biel, M., & Kleppisch, T. (2011). HCN2 channels in local inhibitory interneurons constrain LTP in the hippocampal direct perforant path. *Cellular and Molecular Life Sciences*, *68*, 125–137. https://doi.org/10.1007/s00018-010-0446-z

Muller, C., & Remy, S. (2014). Dendritic inhibition mediated by O-LM and bistratified interneurons in the hippocampus. *Frontiers in Synaptic Neuroscience*, *6*, 1–15. https://doi.org/10.3389/fnsyn.2014.00023

Murray, A. J., Sauer, J.-F., Riedel, G., McClure, C., Ansel, L., Cheyne, L., Bartos, M., Wisden, W., & Wulff, P. (2011). Parvalbumin-positive CA1 interneurons are required for spatial working but not for reference memory. *Nature Neuroscience*, *14*, 297–299. https://doi.org/10.1038/nn.2751

Ordemann, G. J., Apgar, C. J., & Brager, D. H. (2019). D-type potassium channels normalize action potential firing between dorsal and ventral CA1 neurons of the mouse hippocampus. *Journal of Neurophysiology*, *121*, 983–995. https://doi.org/10.1152/jn.00737.2018

Pelkey, K. A., Chittajallu, R., Craig, M. T., Tricoire, L., Wester, J. C., & McBain, C. J. (2017). Hippocampal GABAergic Inhibitory Interneurons. *Physiological Reviews*, *97*, 1619–1747. https://doi.org/10.1152/physrev.00007.2017

Peters, H. C., Hu, H., Pongs, O., Storm, J. F., & Isbrandt, D. (2005). Conditional transgenic suppression of M channels in mouse brain reveals functions in neuronal excitability, resonance and behavior. *Nature Neuroscience*, *8*, 51–60. https://doi.org/10.1038/nn1375

Royer, S., Zemelman, B. V., Losonczy, A., Kim, J., Chance, F., Magee, J. C., & Buzsáki, G. (2012). Control of timing, rate and bursts of hippocampal place cells by dendritic and somatic inhibition. *Nature Neuroscience*, *15*, 769–775. https://doi.org/10.1038/nn.3077

Sik, A., Penttonen, M., Ylinen, A., & Buzsaki, G. (1995). Hippocampal CA1 interneurons: An in vivo intracellular labeling study. *Journal of Neuroscience*, *15*, 6651–6665.

Sik, A., Ylinen, A., Penttonen, M., & Buzsaki, G. (1994). Inhibitory CA1-CA3-hilar region feedback in the hippocampus. *Science*, *265*, 1722–1724. https://doi.org/10.1126/science.8085161

Taniguchi, H., He, M., Wu, P., Kim, S., Paik, R., Sugino, K., Kvitsani, D., Fu, Y., Lu, J., Lin, Y., Miyoshi, G., Shima, Y., Fishell, G., Nelson, S. B., & Huang, Z. J. (2011). A resource of cre driver lines for genetic targeting of GABAergic neurons in cerebral cortex. *Neuron*, *71*, 995–1013. https://doi.org/10.1016/j.neuron.2011.07.026

Tricoire, L., Pelkey, K. A., Erkkila, B. E., Jeffries, B. W., Yuan, X., & McBain, C. J. (2011). A blueprint for the spatiotemporal origins of mouse hippocampal interneuron diversity. *Journal of Neuroscience*, *31*, 10948–10970. https://doi.org/10.1523/JNEUROSCI.0323-11.2011

Williams, S. R., & Stuart, G. J. (2003). Voltage- and site-dependent control of the somatic impact of dendritic IPSPs. *Journal of Neuroscience*, *23*, 7358–7367. https://doi.org/10.1523/JNEUROSCI.23-19-07358.2003

Winterer, J., Lukacsovich, D., Que, L., Sartori, A. M., Luo, W., & Földy, C. (2019). Single-cell RNA-Seq characterization of anatomically identified OLM interneurons in different transgenic mouse lines. *European Journal of Neuroscience*, *50*(11), 3750–3771. https://doi.org/10.1111/ejn.14549

Zemankovics, R., Káli, S., Paulsen, O., Freund, T. F., & Hájos, N. (2010). Differences in subthreshold resonance of hippocampal pyramidal cells and interneurons: The role of h-current and passive membrane characteristics. *The Journal of Physiology*, *588*, 2109–2132.

How to cite this article: Hewitt LT, Ordemann GJ, Brager DH. High and low expression of the hyperpolarization activated current (I_h) in mouse CA1 stratum oriens interneurons. *Physiol Rep*. 2021;9:e14848. https://doi.org/10.14814/phy2.14848